1 **Virus-derived peptide inhibitors of the herpes simplex virus type 1 nuclear egress complex**

2

3 *Elizabeth B. Draganova[1] and Ekaterina E. Heldwein[1,*]*

4 [1]Department of Molecular Biology and Microbiology, Tufts University School of Medicine,

5 Boston, MA, 02111, USA

6

7 [*]Correspondence: Ekaterina Heldwein, Tufts University School of Medicine, 136 Harrison

8 Avenue, Boston, MA 02111; 617-636-0858; katya.heldwein@tufts.edu

9

Abstract

Herpesviruses infect a majority of the human population, establishing lifelong latent infections for which there is no cure. Periodic viral reactivation spreads infection to new hosts while causing various disease states particularly detrimental in the immunocompromised. Efficient viral replication, and ultimately the spread of infection, is dependent on the nuclear egress complex (NEC), a conserved viral heterodimer that helps translocate mature viral capsids from the nucleus to the cytoplasm where they mature into infectious virions. Here, we have identified peptides capable of inhibiting the membrane-budding activity of the NEC *in vitro*. Biophysical characterization of these peptides using circular dichroism suggests that secondary structure, rather than amino acid sequence, influences the extent of inhibition. Current therapeutics that target viral DNA replication machinery are rendered ineffective by drug resistance due to viral mutations. Our results establish a basis for the development of an alternative class of inhibitors against nuclear egress, an essential step in herpesvirus replication, potentially expanding the current repertoire of available therapeutics.

24 The design of novel antiviral therapeutics is a rapidly expanding field because viruses remain
25 one of the most common causes of human disease. One important group of viral human
26 pathogens are herpesviruses that infects a majority of the population by establishing lifelong
27 dormant infections for which there is no cure (reviewed in [1-3]). Periodically, the virus reactivates,
28 resulting in diseases such as keratitis, blindness, and cancers, which pose a significant threat to
29 immunocompromised individuals. Current antiviral treatments of choice are nucleoside analogs
30 such as acyclovir that target DNA replication machinery; yet, viral resistance to these drugs
31 renders them ineffective, highlighting the need for additional therapeutics[4-6].
32 The spread of infection to uninfected tissues and hosts relies on the ability of the virus to
33 effectively replicate[2,7]. During replication, viral capsids are assembled within the nucleus and
34 must translocate into the cytoplasm to form infectious virions but are too large to traverse
35 nuclear pores, and instead use an unusual route termed nuclear egress. The first step in this
36 process is the budding of a capsid at the inner nuclear membrane (INM), which is mediated by
37 the conserved nuclear egress complex (NEC), a heterodimer of viral proteins UL31 and
38 UL34[2,7,8]. The NEC is anchored to the INM by the single C-terminal transmembrane helix of
39 UL34[9]. UL31 colocalizes with UL34[10,11] so that the complex extends outward into the
40 nucleoplasm where UL31 binds capsids ready for egress[12,13].
41 Our group has demonstrated that purified recombinant NEC expressed in *E. coli*
42 vesiculates synthetic membranes (giant unilamellar vesicles; GUVs) in the absence of other
43 proteins or ATP[14]. Using cryo-electron microscopy and tomography (cryo-EM/ET), we showed
44 that during budding, NEC oligomerizes into hexagonal membrane-bound coats[14]. We also found
45 that HSV-1 NEC formed a hexagonal lattice of similar dimensions in crystals, which reinforced
46 the inherent ability of the complex to form hexagonal arrays and provided an atomic-level view

47 of protein interactions within the coat[15]. Mutations intended to disrupt hexagonal lattice
48 formation impaired NEC-mediated budding *in vitro* and reduced nuclear egress and viral
49 replication *in vivo*[16,17], which confirmed that NEC oligomerization is essential for the NEC
50 function. Furthermore, removal of NEC regions required for binding membranes *in vitro*[14] also
51 reduced viral replication *in vivo*[18,19], suggesting that appropriate membrane interactions are also
52 required for budding. Therefore, NEC-mediated budding is as an attractive therapeutic target.
53 Recently, we showed that HSV-1 NEC-mediated budding could be inhibited *in vitro* by
54 another HSV-1 protein, capsid protein UL25[20]. UL25 is located at the capsid vertices and is
55 thought to anchor the NEC to the capsid during nuclear egress[13,21]. We found that an N-
56 terminally truncated UL25 construct UL25Δ44 Q72A (Fig. 1) inhibited NEC budding at a 10:1
57 molar ratio of UL25:NEC[20]. Using cryo-ET, we showed that the observed inhibitory effect on
58 NEC budding correlated with a network of interconnected UL25 stars formed on top of the
59 membrane-bound NEC layer. We hypothesized that this UL25 network blocked budding by
60 preventing the conformational changes within the NEC necessary to generate membrane
61 deformation and budding. UL25-mediated budding inhibition required the N-terminal α-helix in
62 UL25, residues 45-94 (Fig. 1a), as a UL25Δ73 construct in which the N-terminal ~1/2 of this
63 helix was truncated did not inhibit budding. We then tested whether peptides derived from the N-
64 terminal α-helix of UL25 could inhibit NEC-mediated budding. Here, we show that UL25-
65 derived peptides inhibit NEC budding and identify structural characteristics essential for
66 inhibition.
67
68 **Results**
69 **UL25-derived peptides inhibit NEC budding, in a dose-dependent, length-dependent, but**
70 **sequence-independent manner.** We first tested whether the peptide corresponding to the entire

71 N-terminal helix of UL25, UL25$^{native(45-94)}$ (Fig. 1b), inhibited NEC-mediated budding in an
72 established *in-vitro* GUV budding assay[14] (Fig. 2a, b). NEC and UL25$^{native(45-94)}$ were added to
73 GUVs in 1:0.1, 1:0.3, 1:0.6, 1:1 and 1:10 molar ratios of NEC:peptide, and budding efficiency
74 was quantified. We found that the UL25$^{native(45-94)}$ peptide inhibited NEC budding in a dose-
75 dependent manner and that the maximal inhibitory effect, a ~75% reduction in budding, was
76 achieved at a 1:1 molar ratio of NEC:peptide (Fig. 2c). Surprisingly, a scrambled UL25$^{scr(45-94)}$
77 peptide (Fig. 1b) inhibited budding with a similar efficiency (Fig. 2c), which suggested that the
78 native UL25 peptide sequence was unimportant for the inhibitory activity. By contrast, a shorter
79 UL25$^{74-94}$ peptide (Fig. 1b) had a weak inhibitory effect on budding at a 1:1 or 1:10 molar ratios,
80 ~25%, which was not statistically significant (Fig. 2c). Therefore, the inhibitory activity of the
81 UL25-derived peptides is length-dependent.
82 UL25Δ44 Q72A, which served as a control, was not inhibitory at a 1:1 molar ratio (Fig.
83 2c), in agreement with our previous findings[20]; yet at a 1:10 molar ratio of NEC:UL25, it reduced
84 NEC budding by ~90% (Fig. 2c). The differences in inhibition between UL25 and UL25-derived
85 peptides are likely due to distinct inhibitory mechanisms.
86
87 **The ability of the peptides to form α-helical structure correlates with inhibition of NEC-**
88 **mediated budding.** Within capsid-bound UL25, amino acids 48-94 form an α-helix (Fig. 1a).
89 Yet, the circular dichroism (CD) spectra of both the UL25$^{native(45-94)}$ and the UL25$^{scr(45-94)}$ peptides
90 lacked any obvious α-helical signature in solution (Fig. 3a, b) and were only ~10% α-helical
91 according to the estimates using DichroWeb[23] (Supplementary Table S1). To assess the
92 propensity of the UL25 peptides to form α-helical structure under certain conditions, the CD
93 experiment was repeated in the presence of 30% trifluoroethanol (TFE), which is known to

94 stabilize secondary structure[24]. In the presence of TFE, spectra of both peptides had clear α-
95 helical structure (Fig. 3a, b), ~37% and ~31%, respectively (Supplementary Table S1),
96 suggesting that each peptide could, in principle, form an α-helix in the proper environment, for
97 example, when bound to a protein partner such as the NEC. The $\theta_{222}/\theta_{208}$ ratios of both peptides
98 either in the absence or the presence of TFE were < 0.9 indicating peptides were forming
99 individual helices rather than coiled coils[25].
100 The shorter UL25$^{scr(74-94)}$ peptide adopted a random-coil conformation in solution even in
101 the presence of 30% TFE (Fig. 3c, Supplementary Table 1). Therefore, it may be unable to
102 inhibit NEC budding to a similar extent as the longer UL25$^{native(45-94)}$ and the UL25$^{scr(45-94)}$ peptides
103 because it cannot form an α-helix.
104
105 **A pre-formed α-helical peptide moderately inhibits budding whereas a random-coil peptide**
106 **does not**. The inhibitory UL25-derived peptides can form α-helical structure whereas the non-
107 inhibitory peptide does not, implying a correlation between the two properties. However, the
108 inhibitory peptides are also substantially longer than the non-inhibitory one. Therefore, to
109 explore the apparent correlation between the propensity to form an α-helix and the ability to
110 inhibit NEC-mediated budding while ruling out the peptide length as a variable, we tested two
111 heterologous peptides: a 50-amino-acid sequence from HSV-1 glycoprotein B (gB$^{103-152}$), which
112 lacks any regular secondary structure in the crystal structure[26] and a 53-amino-acid peptide
113 containing a series of well-characterized α-helical EAEKAAK repeats [$(EAEKAAK)_7$EAEK][27]
114 (Fig. 1b). The gB$^{103-152}$ peptide was not inhibitory at a 1:1 molar ratio of NEC:peptide (Fig. 2c)
115 and only had a weak inhibitory effect on budding at a 1:10 molar ratio of NEC:peptide, ~25%,
116 which was not statistically significant (Fig. 2c). CD analysis showed this peptide adopted a

117 random-coil conformation in solution even in the presence of 30% TFE (Fig. 3d, Supplementary
118 Table 1). These observations suggest that the ability of the peptides to form an α-helix is
119 important for their inhibitory activity.

120 The $(EAEKAAK)_7EAEK$ peptide was 60% α-helical in solution even in the absence of
121 TFE (Fig. 3e, Supplementary Table 1), in contrast to both the $UL25^{native(45-94)}$ and the $UL25^{scr(45-94)}$
122 peptides that became mostly α-helical only in the presence of TFE (Fig. 3a, b). Yet, it was not
123 inhibitory at a 1:1 molar ratio of NEC:peptide and moderately inhibited NEC-mediated budding
124 at a 1:10 molar ratio, by ~50% (Fig. 2c). The differences in the inhibitory activities of the three
125 peptides that can form α-helices could be due to different amino acid composition, especially,
126 the charged residue content. The $(EAEKAAK)_7EAEK$ peptide contains 60% charged residues
127 (glutamates and lysines) whereas the UL25-derived inhibitory peptides contain only 30%
128 charged residues (aspartates, glutamates and arginines). The moderate inhibitory activity of the
129 $(EAEKAAK)_7EAEK$ peptide at high concentrations could be due to its non-specific interactions
130 with the NEC due to high charge. Alternatively, optimal inhibition may require a peptide that
131 forms an α-helix in the presence of the NEC, perhaps, in an induced-fit manner, instead of a
132 stable, pre-formed α-helix.

133

134 **Inhibitory peptides do not block NEC/membrane interactions.** Peptides could inhibit NEC-
135 mediated budding by preventing the NEC from binding to membranes. We first tested whether
136 the peptides themselves could bind multilamellar vesicles (MLVs) of the same lipid composition
137 as the GUVs used in the budding assay and found that none did (Fig. 4). This suggested that the
138 peptides do not compete with the NEC for binding to membranes. We then tested whether the
139 inhibitory peptides could block the NEC from binding to membranes.

140 To assess if the NEC could bind membranes in presence of inhibitory peptides, we
141 performed a co-sedimentation assay with NEC, MLVs, and either $UL25^{native(45-94)}$ or $UL25^{scr(45-94)}$.
142 UL25Δ44 Q72A, which inhibits budding but does not prevent the NEC from binding
143 membranes[20], was used as a control. Experiments were performed at a 1:10 molar ratio of
144 NEC:peptide or NEC:UL25 molar ratio because the UL25Δ44 Q72A control inhibits at a 1:10
145 molar ratio of NEC:UL25. We found that neither peptide prevented the NEC from binding
146 membranes as judged by the same amount of MLV-bound NEC (~95%) in the absence or the
147 presence of peptides (Fig. 5). As expected[20], UL25Δ44 Q72A also did not block NEC membrane
148 binding (Fig. 5). Thus, the inhibitory peptides do not block NEC/membrane interactions and,
149 instead, inhibit NEC budding by some other mechanism.
150

151 **Discussion**

152 Here, we have shown that two peptides derived from the N-terminal α-helix of UL25
153 efficiently inhibited NEC-mediated budding *in vitro* in a dose-dependent manner. The inhibitory
154 ability of the peptides depended on their length and the ability to form an α-helix but not on the
155 exact amino acid sequence. Peptide length was more important for inhibition than the sequence
156 because 50-amino-acid UL25 peptides, be they native or scrambled ($UL25^{native(45-94)}$ and $UL25^{scr(45-}$
157 $^{94)}$), efficiently inhibited budding whereas the 21-amino-acid native peptide $UL25^{74-94}$ did not.
158 Future studies will identify the minimal UL25 peptide length required for inhibition. The
159 inhibitory ability of UL25 peptides correlated not only with their length but also with the
160 propensity to adopt α-helical structure. Although all three UL25-derived peptides formed
161 random coils in solution, the two 50-amino-acid peptides formed α-helices in the presence of
162 TFE, known to stabilize secondary structure, but the 21-amino-acid native peptide did not.

163 To uncouple the propensity to form α-helices from the peptide length, we tested a
164 heterologous 50-amino-acid peptide from HSV-1 gB ($gB^{103-152}$) that lacks any regular secondary
165 structure in the crystal structure[26]. We confirmed that this peptide formed a random coil and
166 showed that had a weak inhibitory activity only at high molar ratios of NEC:peptide.
167 We also tested a heterologous 53-amino-acid peptide containing a series of well-characterized α-
168 helical EAEKAAK repeats [$(EAEKAAK)_7EAEK$][27]. We found that, unlike the inhibitory UL25-
169 derived peptides, this peptide was α-helical in solution even in the absence of TFE and that it had
170 a modest inhibitory effect only at the highest molar ratio of NEC:peptide. This heterologous α-
171 helical peptide is highly charged and forms an amphipathic α-helix with a charged face rich in
172 glutamates and lysines and a hydrophobic face rich in alanines (Supplementary Fig. S2). In
173 contrast, inhibitory UL25-derived peptides are less charged and form α-helices with a less
174 pronounced amphipathic character (Supplementary Fig. S2). The moderate inhibitory activity of
175 the $(EAEKAAK)_7EAEK$ peptide at high concentrations could be due to its non-specific
176 interactions with the NEC. Alternatively, it is possible that a stable, preformed α-helix may not
177 be able to form appropriate inhibitory contacts with the NEC and that for efficient inhibition, an
178 α-helix of a specific length and amino-acid content should form in the presence of the NEC, in
179 an induced-fit manner. Therefore, future design of NEC peptide inhibitors should take both of
180 these characteristics into consideration.
181 The mechanism by which the inhibitory peptides inhibit budding is yet unclear. Our data
182 suggest that the inhibitory peptides do not prevent the NEC from binding the membranes.
183 Therefore, we hypothesize that the peptides may, instead, inhibit the membrane-budding activity
184 of the NEC by some other mechanism, for example, by blocking NEC/NEC interactions required
185 for budding or prevent conformational changes required by the NEC to undergo budding (Fig. 6).

186 Our previous study suggested that UL25 inhibited NEC-mediated budding by
187 oligomerizing into a network of interconnected stars on top of the membrane-bound NEC layer
188 as observed by cryo-ET[20]. We hypothesized that the N-terminal helices link the neighboring
189 UL25 molecules into a network by forming antiparallel helical bundles that sterically blocked the
190 NEC from undergoing conformational changes necessary for membrane budding. Both the N-
191 terminal helix and the C-terminal core of UL25 (Fig. 1a) were important for inhibition. However,
192 the inhibitory UL25 peptides in our current study were composed of only the N-terminal helix.
193 Therefore, they likely bind the NEC differently from UL25 and use a different mechanism to
194 inhibit budding. Being much smaller than UL25, the inhibitory peptides can interact with the
195 NEC at sites otherwise inaccessible to the UL25 protein. Alternatively, NEC/peptide interactions
196 may block NEC/NEC interactions necessary for the assembly of the hexagonal NEC coat thereby
197 blocking the induction of negative curvature and, ultimately, budding (Fig. 6). Additional
198 experiments, such as fluorescent labeling of the peptides, are necessary to show peptide binding
199 to membrane-bound NEC.
200 Our results suggest that inhibitory peptides should be of a certain length, moderately
201 charged, and unstructured in solution, yet capable of forming α-helical structure, presumably,
202 upon binding to the NEC. Further structural analyses of the inhibitory peptides in the presence of
203 the NEC are necessary to narrow down the optimal characteristics of the inhibitory peptides,
204 including their delivery to their intracellular target. The length of the inhibitory peptides
205 identified in this study, 50 amino acids, presents challenges for intracellular delivery. Most
206 therapeutic peptides are ~20-30 amino acids in length, which increases the likelihood of crossing
207 the plasma membrane, yet many require additional alterations of their physical properties to do
208 so[28]. Furthermore, peptides are susceptible to proteolytic degradation and can exhibit off-target

209 effects in cells, both of which the likelihood increasing the longer the peptide, reducing the
210 chances of binding the intended target. Therefore, determining the minimal inhibitory length of
211 these peptides will be essential for transitioning from *in-vitro* to *in-vivo* studies. Lastly, the NEC
212 is located within the nucleus, requiring inhibitory peptides to not only reach the cytoplasm but
213 also enter the nucleus. A recent peptide cellular localization assay showed that peptides smaller
214 than 40 kDa can diffuse through the nuclear pore[29], suggesting NEC inhibitory peptides could do
215 so as well.

216 Efficient NEC function is required for successful replication of herpesviruses. To our
217 knowledge, this is the first study reporting a peptide-based approach targeting NEC budding. Our
218 work provides a starting point for the rational design of peptide-based inhibitors of the NEC and
219 nuclear egress. Both the NEC and UL25 are conserved across all herpesviruses raising an
220 intriguing possibility that UL25-derived peptides could be used to inhibit NEC homologs from
221 other herpesviruses.

222

223 **Materials and Methods**

224 ***Peptides.*** All peptides used in this study were purchased from Peptide 2.0 with the exception of
225 the α-helical $(EAEKAAK)_7EAEK$ peptide, which was cloned, expressed and purified as
226 described below.

227

228 ***Cloning.*** All primers used in cloning are listed in Supplementary Table S2. The DNA sequence
229 encoding the α-helical [$(EAEKAAK)_7EAEK$] peptide was subcloned into the prokaryotic
230 expression vector pGEX-6P-1 that encodes a N-terminal GST-tag followed by a PreScission
231 Protease cleavage site in frame with the BamHI restriction site within the multiple cloning site.

232 The $(EAEKAAK)_7EAEK$ peptide DNA sequence was obtained as a gBlock gene fragment (IDT)
233 and subjected to restriction digest cloning with BamHI and XhoI into the pGEX-6P-1 vector (the
234 gene fragment sequence is listed in Supplementary Table S2) to create the pED39 [$(EAEKAAK)$
235 $_7EAEK$ peptide] plasmid.
236
237 ***Expression and purification of NEC220.*** Plasmids encoding HSV-1 UL31 1-306 (pKH90) and
238 UL34 1-220 (pJB02) were co-transformed into *Escherichia coli* BL21(DE3) LoBSTr cells
239 (Kerafast) to generate NEC220 (NEC construct absent of the UL34 C-terminal transmembrane
240 helix)[14]. NEC220 was expressed using autoinduction at 37 °C in Terrific Broth (TB)
241 supplemented with 100 μg/mL kanamycin, 100 μg/mL ampicillin, 0.2% lactose, and 2 mM
242 $MgSO_4$ for 4 h. The temperature was then reduced to 25 °C for 16 h. Cells were harvested at
243 5,000 x g for 30 min. NEC220 was purified as previously described[14] with slight modifications.
244 NEC220 was passed over 2 x 1 mL HiTrap Talon columns (GE Healthcare), rather than ion
245 exchange, to remove excess cleaved His_6-SUMO before injection onto size-exclusion
246 chromatography.
247
248 ***Expression and purification of UL25Δ44 Q72A.*** The plasmid encoding HSV-1 UL25Δ44 Q72A
249 (pED03) was expressed and cells harvested as described above for NEC220 except that only 100
250 μg/mL kanamycin was used. UL25Δ44 Q72A was purified as previously described[20].
251
252 ***Expression and purification of $(EAEKAAK)_7EAEK$.*** The plasmid encoding the peptide sequence
253 was expressed and cells harvested as described above for the NEC220 with the exception that
254 only 100 μg/mL ampicillin was used. Cells were resuspended in lysis buffer (50 mM Na HEPES

255 pH 7.5, 500 mM NaCl, 1 mM TCEP, and 10% glycerol) plus Complete protease inhibitor
256 (Roche) and lysed using a microfluidizer 110S (Microfluidics). The cell lysate was centrifuged at
257 13,000 x g for 35 min, and the supernatant passed over a Glutathione sepharose 4B (GE
258 Healthcare) column, which was subsequently washed with lysis buffer. The GST-tag was
259 cleaved on the glutathione sepharose column for 16 h using the PreScission Protease described
260 above. The peptide was eluted off the column with lysis buffer. As a final purification step, the
261 peptide was purified with size-exclusion chromatography using a Superdex 75 column (GE
262 Healthcare) equilibrated with gel filtration buffer (20 mM Na HEPES, pH 7.0, 100 mM NaCl,
263 and 1 mM TCEP) for budding assays or with CD buffer (10 mM sodium phosphate, pH 7.4, and
264 100 mM NaF) for CD studies. Absorbance was monitored at 214 nm because the peptide lacks
265 aromatic residues. The peptide was purified to homogeneity as assessed by both 16.5% Tris-
266 Tricine SDS-PAGE and 12% SDS-PAGE with Coomassie staining. Fractions containing peptide
267 were concentrated and sent off for amino acid analysis (University of Colorado Denver Anschutz
268 Medical Campus) for accurate concentration determination.
269
270 ***Co-sedimentation assays.*** Co-sedimentation of either peptides alone or NEC and peptides (1:10
271 molar ratio of NEC:peptide) to multilamellar vesicles (MLVs) was performed as previously
272 described[14]. MLVs were prepared in a 3:1:1 molar ratio of 1-palmitoyl-2-oleoyl-glycero-3-
273 phosphocholine (POPC):1-palmitoyl-2-oleoyl-sn-glycero-3-phospho-L-serine (POPS):1-
274 palmitoyl-2-oleoyl-sn-glycero-3-phosphate (POPA) (Avanti Polar Lipids). Background signal in
275 the absence of liposomes is due to protein aggregation during centrifugation. Each experiment
276 was done in three biological replicates with two technical replicates. For peptides alone, the
277 reported values represent the average binding of each biological replicate of peptide to MLVs

278 relative to the NEC (100%). For experiments measuring NEC/MLV binding in the presence of
279 peptides, reported values represent the percentage (0-100%) of co-sedimentation of either
280 NEC220 or peptides in the absence or presence of MLVs. The standard error of the mean is
281 reported for each measurement.
282
283 ***GUV Budding Assays.*** Giant unilamellar vesicles (GUVs) were prepared as previously
284 described[14]. For NEC220 only budding quantification, a total of 10 μL of GUVs with a 3:1:1
285 molar ratio of POPC:POPS:POPA containing ATTO-594 DOPE (ATTO-TEC GmbH) at a
286 concentration of 0.2 μg/μL was mixed with 1 μM NEC220 (final concentration), and 0.2 mg/mL
287 (final concentration) Cascade Blue Hydrazide (ThermoFisher Scientific). For the NEC and
288 peptide experiments, 10 μL of GUVs and 0.1, 0.3, 0.6, 1, or 10 μM (final concentration) of either
289 the $UL25^{native(45-94)}$, $UL25^{scr(45-94)}$, $UL25^{74-94}$, $gB^{103-152}$, or $(EAEKAAK)_7EAEK$ peptides were
290 incubated with 1 μM of NEC220 (final concentration) along with Cascade blue. The total
291 volume of each sample during imaging for all experiments was brought to 100 μL with the gel
292 filtration buffer and the reaction was incubated for 5 min at 20 °C. Samples were imaged in a 96-
293 well chambered cover-glass. Images were acquired using a Nikon A1R Confocal Microscope
294 with a 60x oil immersion lens at the Tufts Imaging Facility in the Center for Neuroscience
295 Research at Tufts University School of Medicine. Quantification was performed by counting
296 vesicles in 15 different frames of the sample (~300 vesicles total). Each experiment was done in
297 at least three biological replicates, each with three technical replicates. Prior to analysis, the
298 background was subtracted from the raw values. All raw values are given in Supplementary
299 Table S3. The reported values represent the average budding activity relative to NEC220

300 (100%). The standard error of the mean is reported for each measurement. Significance
301 compared to NEC220 was calculated using an unpaired one-tailed *t*-test against NEC220.
302
303 ***Circular dichroism (CD) studies.*** Far-UV CD spectra of peptides (0.1 mg/mL) were recorded in
304 10 mM Na phosphate, pH 7.4, and 100 mM NaF buffer using a Jasco 815 CD Spectropolarimeter
305 at the Center for Macromolecular Interactions at Harvard Medical School. Peptide spectra were
306 also measured in the presence of 30% trifluoroethanol (TFE). Data were collected at ambient
307 temperature with a scan speed of 50 nm/min and 5 accumulations of each sample was averaged.
308 The raw data was blank subtracted and converted to mean residue ellipticity (MRE). Helical
309 content was estimated using DichroWeb[23], and average values from three reference datasets
310 generated by the same analysis program are provided in Supplementary Table S1.
311

312 **References**
313

314 1. Johnson, D. C. & Baines, J. D. Herpesviruses remodel host membranes for virus egress.
315 *Nat. Rev. Microbiol.* **9**, 382-394, doi:10.1038/nrmicro2559 (2011).

316 2. Bigalke, J. M. & Heldwein, E. E. Nuclear exodus: Herpesviruses lead the way. *Annu.*
317 *Rev. Virol.* **3**, 387-409, doi:10.1146/annurev-virology-110615-042215 (2016).

318 3. Mettenleiter, T. C., Klupp, B. G. & Granzow, H. Herpesvirus assembly: an update. *Virus*
319 *Res.* **143**, 222-234, doi:10.1016/j.virusres.2009.03.018 (2009).

320 4. Szczubialka, K., Pyrc, K. & Nowakowska, M. In search for effective and definitive
321 treatment of herpes simplex virus type 1 (HSV-1) infections. *RSC Adv.* **6**, 1058-1075,
322 doi:10.1039/c5ra22896d (2016).

323 5. Engel, J. P., Englund, J. A., Fletcher, C. V. & Hill, E. L. Treatment of resistant herpes
324 simplex virus with continuous-infusion acyclovir. *JAMA.* **263**, 1662-1664 (1990).

325 6. Antoine, T. E., Park, P. J. & Shukla, D. Glycoprotein targeted therapeutics: a new era of
326 anti-herpes simplex virus-1 therapeutics. *Rev. Med. Virol.* **23**, 194-208,
327 doi:10.1002/rmv.1740 (2013).

328 7. Draganova, E. B., Thorsen, M. K. & Heldwein, E. E. Nuclear Egress. *Curr. Issues Mol.*
329 *Biol.* **41**, 125-170, doi:10.21775/cimb.041.125 (2020).

330 8. Reynolds, A. E., Wills, E. G., Roller, R. J., Ryckman, B. J. & Baines, J. D. Ultrastructural
331 localization of the herpes simplex virus type 1 UL31, UL34, and US3 proteins suggests
332 specific roles in primary envelopment and egress of nucleocapsids. *J. Virol.* **76**, 8939-
333 8952 (2002).

334 9. Shiba, C. *et al.* The UL34 gene product of herpes simplex virus type 2 is a tail-anchored
335 type II membrane protein that is significant for virus envelopment. *J. Gen. Virol.* **81**,
336 2397-2405, doi:10.1099/0022-1317-81-10-2397 (2000).

337 10. Reynolds, A. E. *et al.* U(L)31 and U(L)34 proteins of herpes simplex virus type 1 form a
338 complex that accumulates at the nuclear rim and is required for envelopment of
339 nucleocapsids. *J. Virol.* **75**, 8803-8817 (2001).

340 11. Chang, Y. E. & Roizman, B. The product of the UL31 gene of herpes simplex virus 1 is a
341 nuclear phosphoprotein which partitions with the nuclear matrix. *J. Virol.* **67**, 6348-6356
342 (1993).

343 12. Trus, B. L. *et al.* Allosteric signaling and a nuclear exit strategy: binding of UL25/UL17
344 heterodimers to DNA-Filled HSV-1 capsids. *Mol. Cell.* **26**, 479-489,
345 doi:10.1016/j.molcel.2007.04.010 (2007).

346 13. Yang, K. & Baines, J. D. Selection of HSV capsids for envelopment involves interaction
347 between capsid surface components pUL31, pUL17, and pUL25. *Proc. Natl. Acad. Sci.*
348 **108**, 14276-14281, doi:10.1073/pnas.1108564108 (2011).

349 14. Bigalke, J. M., Heuser, T., Nicastro, D. & Heldwein, E. E. Membrane deformation and
350 scission by the HSV-1 nuclear egress complex. *Nat. Commun.* **5**, 4131,
351 doi:10.1038/ncomms5131 (2014).

352 15. Bigalke, J. M. & Heldwein, E. E. Structural basis of membrane budding by the nuclear
353 egress complex of herpesviruses. *EMBO J.* **34**, 2921-2936,
354 doi:10.15252/embj.201592359 (2015).

355 16. Roller, R. J., Zhou, Y., Schnetzer, R., Ferguson, J. & DeSalvo, D. Herpes simplex virus
356 type 1 U(L)34 gene product is required for viral envelopment. *J. Virol.* **74**, 117-129
357 (2000).

358 17. Fuchs, W., Klupp, B. G., Granzow, H., Osterrieder, N. & Mettenleiter, T. C. The
359 interacting UL31 and UL34 gene products of pseudorabies virus are involved in egress
360 from the host-cell nucleus and represent components of primary enveloped but not
361 mature virions. *J. Virol.* **76**, 364-378 (2002).

362 18. Mou, F., Wills, E. & Baines, J. D. Phosphorylation of the U(L)31 protein of herpes
363 simplex virus 1 by the U(S)3-encoded kinase regulates localization of the nuclear
364 envelopment complex and egress of nucleocapsids. *J. Virol.* **83**, 5181-5191,
365 doi:10.1128/jvi.00090-09 (2009).

366 19. Passvogel, L., Trube, P., Schuster, F., Klupp, B. G. & Mettenleiter, T. C. Mapping of
367 sequences in Pseudorabies virus pUL34 that are required for formation and function of
368 the nuclear egress complex. *J. Virol.* **87**, 4475-4485, doi:10.1128/jvi.00021-13 (2013).

369 20. Draganova, E. B., Zhang, J., Zhou, Z. H. & Heldwein, E. E. Structural basis for capsid
370 recruitment and coat formation during HSV-1 nuclear egress. *Elife.* **9**,
371 doi:10.7554/eLife.56627 (2020).

372 21. Yang, K., Wills, E., Lim, H. Y., Zhou, Z. H. & Baines, J. D. Association of herpes
373 simplex virus pUL31 with capsid vertices and components of the capsid vertex-specific
374 complex. *J. Virol.* **88**, 3815-3825, doi:10.1128/jvi.03175-13 (2014).

375 22. DeLano, W., L. The PyMOL Molecular Graphics System, Version 1.7.4 Schrödinger,
376 LLC. http://www.pymol.org (2015).

377 23. Whitmore, L. & Wallace, B. A. Protein secondary structure analyses from circular
378 dichroism spectroscopy: methods and reference databases. *Biopolymers.* **89**, 392-400,
379 doi:10.1002/bip.20853 (2008).

380 24. Luo, P. & Baldwin, R. L. Mechanism of helix induction by trifluoroethanol: a framework
381 for extrapolating the helix-forming properties of peptides from trifluoroethanol/water
382 mixtures back to water. *Biochemistry.* **36**, 8413-8421, doi:10.1021/bi9707133 (1997).

383 25. Lau, S. Y., Taneja, A. K. & Hodges, R. S. Synthesis of a model protein of defined
384 secondary and quaternary structure. Effect of chain length on the stabilization and
385 formation of two-stranded alpha-helical coiled-coils. *J. Biol. Chem.* **259**, 13253-13261
386 (1984).

387 26. Heldwein, E. E. *et al.* Crystal structure of glycoprotein B from herpes simplex virus 1.
388 *Science.* **313**, 217-220, doi:10.1126/science.1126548 (2006).

389 27. Zhou, N. E., Kay, C. M., Sykes, B. D. & Hodges, R. S. A single-stranded amphipathic
390 alpha-helix in aqueous solution: design, structural characterization, and its application for
391 determining alpha-helical propensities of amino acids. *Biochemistry.* **32**, 6190-6197
392 (1993).

393 28. Derakhshankhah, H. & Jafari, S. Cell penetrating peptides: A concise review with
394 emphasis on biomedical applications. *Biomed. Pharmacother.* **108**, 1090-1096,
395 doi:10.1016/j.biopha.2018.09.097 (2018).

396 29. Peraro, L. *et al.* Cell Penetration Profiling Using the Chloroalkane Penetration Assay. *J.*
397 *Am. Chem. Soc.* **140**, 11360-11369, doi:10.1021/jacs.8b06144 (2018).

398

399

400 **Acknowledgments**

401 We would like to thank Shaun Bevers (University of Colorado Denver Biophysics Core) for
402 performing amino acid analysis on the peptides. We also thank Peter Cherepanov (Francis Crick
403 Institute) for the gift of the GST-PreScission protease expression plasmid and Thomas Schwartz
404 (Massachusetts Institute of Technology) for the gift of LoBSTr cells. CD experiments were
405 performed at the Center for Macromolecular Interactions in the Department of Biological
406 Chemistry and Molecular Pharmacology at Harvard Medical School. This work was funded by
407 the NIH grants R01GM111795 and R01AI147625 (E.E.H.), a Faculty Scholar grant 55108533
408 from Howard Hughes Medical Institute (E.E.H.), NIH postdoctoral fellowship F32GM126760
409 (E.B.D.), and NIH IRACDA postdoctoral fellowship K12GM133314 (E.B.D).

410

411 **Author Contributions**

412 E.B.D. and E.E.H. designed the experiments; E.B.D. performed all experiments and analyses
413 under the guidance of E.E.H; E.B.D. and E.E.H. wrote the manuscript.

414

415 **Additional Information**

416 **Competing Interests:** The authors declare no competing interests.

417

418 **Figure Legends**

419 **Figure. 1. Design of UL25-derived peptides. a)** The structure of the full-length, capsid-bound
420 HSV-1 UL25 [residues 1-94 determined by cryo-EM (PDB ID: 6CGR)]; residues 134-580
421 determined by x-ray crystallography (PDB ID: 2F5U)]. The image of the UL25 structure was
422 generated in PyMOL[29]. **b)** Schematic representation of peptides and protein constructs used in

423 inhibition studies. Peptides are indicated by stripes. Amino-acid sequence of each peptide is
424 shown. UL25Δ44 Q72A: N-terminally truncated UL25 mutant, used to yield pure protein;
425 $UL25^{native(45-94)}$: the native N-terminal helix of UL25; $UL25^{scr(45-94)}$: the amino acid sequence of
426 $UL25^{native(45-94)}$ scrambled; $UL25^{74-94}$: the C-terminal half of the $UL25^{native(45-94)}$ peptide; $gB^{103-152}$: a
427 region within the HSV-1 glycoprotein B (gB); $(EAEKAAK)_7EAEK$: a well-characterized α-
428 helical peptide made of EAEKAAK repeats.
429
430 **Figure 2. $UL25^{native(45-94)}$ and $UL25^{scr(45-94)}$ inhibit HSV-1 NEC-mediated budding in a dose-**
431 **dependent manner. a)** A diagram of the NEC-mediated *in-vitro* budding assay generated in
432 Microsoft PowerPoint. The NEC [PDB ID: 4ZXS] binds red fluorescent giant unilamellar
433 vesicles (GUVs) in the presence of the membrane impermeable Cascade Blue dye, inducing
434 negative membrane curvature, and generates intraluminal vesicles (ILVs) filled with Cascade
435 Blue. The number of ILV-containing GUVs serves as a measure of budding efficiency. **b)**
436 Confocal microscopy images show ILVs formed inside the GUVs as the result of the NEC-
437 mediated budding. Fewer ILVs are formed in the presence of $UL25^{native(45-94)}$ or $UL25^{scr(45-94)}$ due to
438 inhibition of budding by the peptides. All images show the red (ATTO-DOPE) and blue
439 (Cascade Blue) channels. Scale bars = 5 μm. **c)** Quantification of the NEC-mediated budding in
440 the absence or the presence of peptides or UL25Δ44 Q72A. Budding was tested at 1:0.1, 1:0.3,
441 1:0.6, 1:1 or 1:10 molar ratios of NEC:UL25 or NEC:peptide. Each experiment was done in three
442 biological replicates, each consisting of three technical replicates. Symbols represent average
443 budding efficiency of each biological replicate relative to NEC220 (100%). Bars show the mean
444 of three biological replicates, with error bars representing the standard error of the mean.

445 Significance compared to NEC220 was calculated using an unpaired *t*-test. *P-value < 0.05, **P-
446 value < 0.01, ***P-value < 0.001, and ****P-value < 0.0001.
447
448 **Figure 3. Secondary structure of the peptides used in this work. a-e)** Far-UV CD spectra of
449 each peptide in the presence of 30% TFE (dashed lines) or in its absence (solid lines). Both the
450 $UL25^{native(45-94)}$ and the $UL25^{scr(45-94)}$ peptides form α-helices in the presence of 30% TFE.
451 $UL25^{74-94}$ and $gB^{103-152}$ are mostly unstructured even in the presence of 30% TFE. The
452 $(EAEKAAK)_7EAEK$ peptide is α-helical regardless of the presence of TFE.
453
454 **Figure 4. Peptides do not bind synthetic liposomes.** NEC but not peptides bind multilamellar
455 vesicles (MLVs) of the same composition as the GUVs used in the in-vitro budding assay.
456 PreScission protease, which does not bind membranes, was used as a negative control. Each
457 experiment was done in three biological replicates, each consisting of two technical replicates.
458 Symbols represent average binding efficiency of each biological replicate relative to NEC220
459 (100%). Bars show the mean of three biological replicates, with error bars representing the
460 standard error of the mean. Significance compared to NEC220 was calculated using an unpaired
461 *t*-test. ****P-value < 0.0001.
462
463 **Figure 5. Peptides do not block membrane binding by the NEC.** Co-sedimentation of
464 NEC220 alone and in the presence of either $UL25^{native(45-94)}$, $UL25^{scr(45-94)}$, or UL25Δ44 Q72A was
465 assessed by a co-sedimentation assay in the presence and absence of MLVs. The amount of co-
466 sedimentation was quantified with Coomassie staining. Bands from representative gels (full gel
467 images are shown in Supplementary Figure 1) used for quantification are boxed and colored as

468 follows: pink – NEC (UL31: 34 kDa and UL34: 25 kDa); green – either UL25$^{native(45-94)}$ (5 kDa) or
469 UL25Δ44 Q72A (57 kDa); blue – UL25$^{scr(45-94)}$) (5 kDa). Each experiment was done in three
470 biological replicates, each consisting of two technical replicates. Symbols represent average
471 binding efficiency of each biological replicate. Bars show the mean of three biological replicates,
472 with error bars representing the standard error of the mean. Significance compared to NEC220 in
473 the presence of MLVs was calculated using an unpaired *t*-test. ****P-value < 0.0001.
474
475 **Figure 6. Proposed model of peptide inhibition of the NEC-mediated budding. a)** NEC
476 (pink) alone binds membranes, induces negative membrane curvature, and generates a budded
477 vesicle containing an internal hexagonal NEC coat. **b)** Both UL25$^{native(45-94)}$ and UL25$^{scr(45-94)}$
478 (bluegreen) inhibit budding by forming α-helices upon binding to the NEC, which likely
479 prevents conformational changes necessary for the formation of the negative membrane
480 curvature. This figure was generated using Biorender (https://biorender.com).

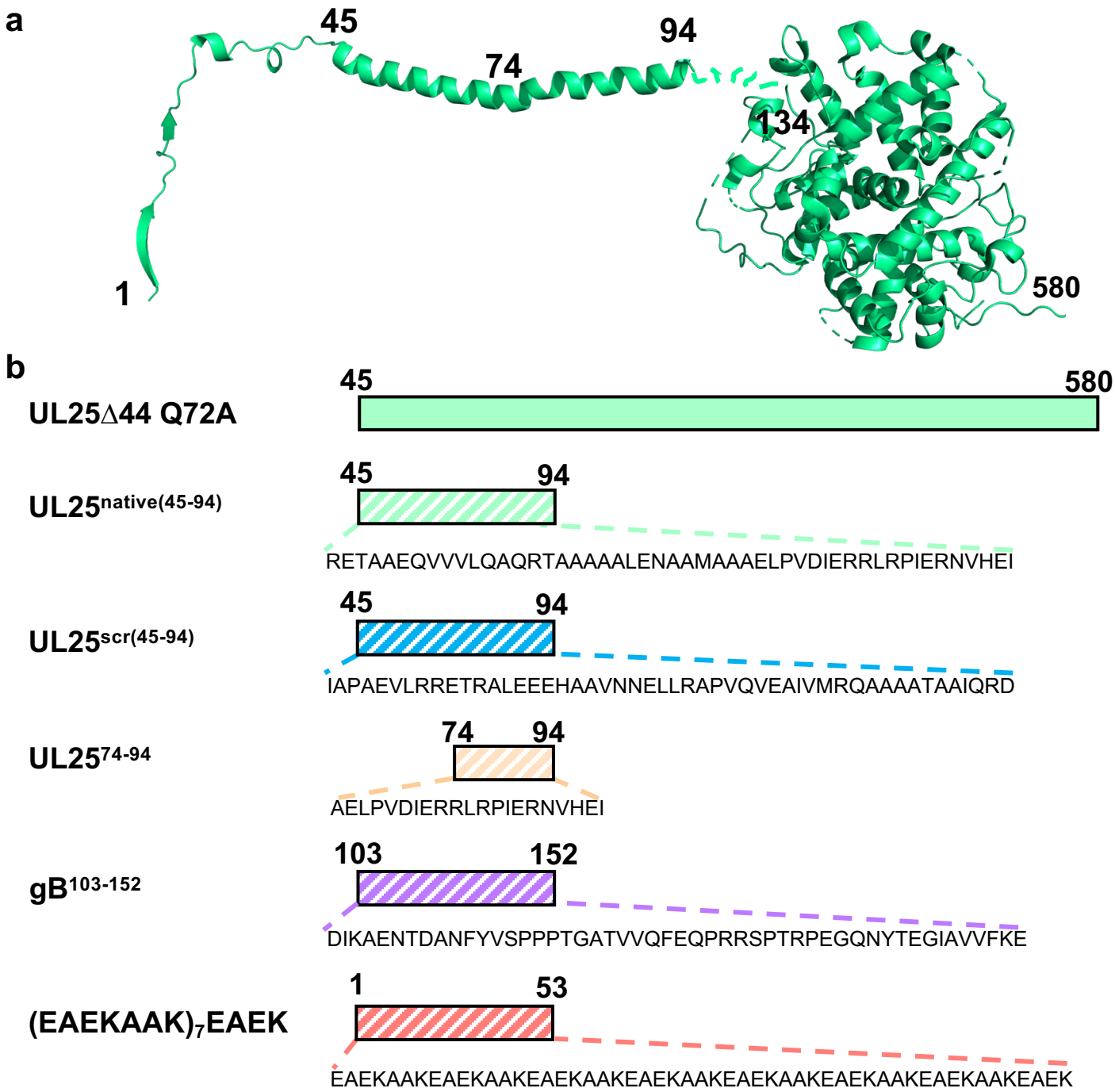

Figure. 1. Design of UL25-derived peptides. a) The structure of the full-length, capsid-bound HSV-1 UL25 [residues 1-94 determined by cryo-EM (PDB ID: 6CGR)]; residues 134-580 determined by x-ray crystallography (PDB ID: 2F5U)]. The image of the UL25 structure was generated in PyMOL. **b)** Schematic representation of peptides and protein constructs used in inhibition studies. Peptides are indicated by stripes. Amino-acid sequence of each peptide is shown. UL25Δ44 Q72A: N-terminally truncated UL25 mutant, used to yield pure protein; $UL25^{native(45-94)}$: the native N-terminal helix of UL25; $UL25^{scr(45-94)}$: the amino acid sequence of $UL25^{native(45-94)}$ scrambled; $UL25^{74-94}$: the C-terminal half of the $UL25^{native(45-94)}$ peptide; $gB^{103-152}$: a region within the HSV-1 glycoprotein B (gB); $(EAEKAAK)_7EAEK$: a well-characterized α-helical peptide made of EAEKAAK repeats.

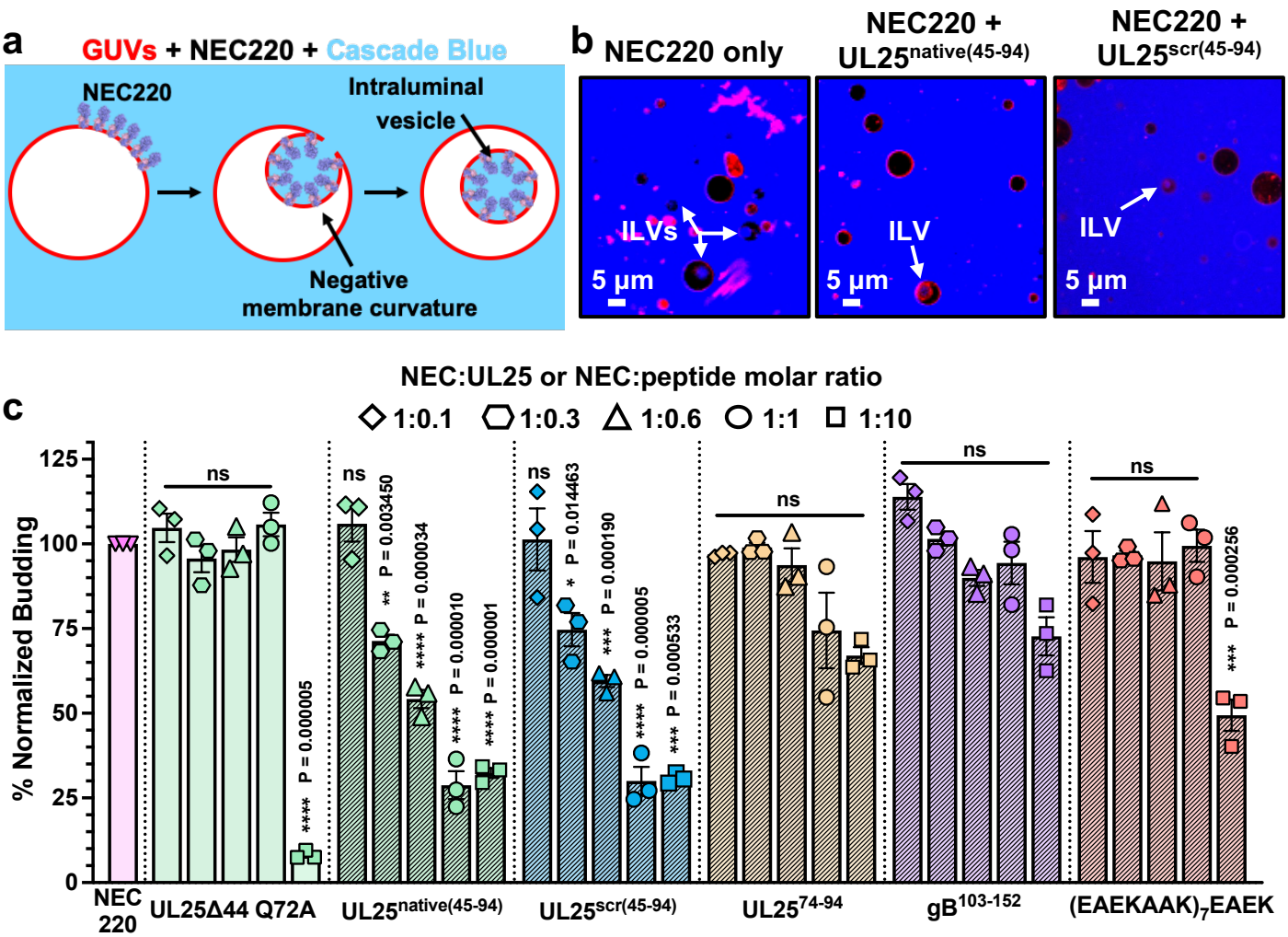

Figure 2. UL25$^{native(45-94)}$ and UL25$^{scr(45-94)}$ inhibit HSV-1 NEC-mediated budding in a dose-dependent manner. a) A diagram of the NEC-mediated *in-vitro* budding assay generated in Microsoft PowerPoint. The NEC [PDB ID: 4ZXS] binds red fluorescent giant unilamellar vesicles (GUVs) in the presence of the membrane impermeable Cascade Blue dye, inducing negative membrane curvature, and generates intraluminal vesicles (ILVs) filled with Cascade Blue. The number of ILV-containing GUVs serves as a measure of budding efficiency. **b)** Confocal microscopy images show ILVs formed inside the GUVs as the result of the NEC-mediated budding. Fewer ILVs are formed in the presence of UL25$^{native(45-94)}$ or UL25$^{scr(45-94)}$ due to inhibition of budding by the peptides. All images show the red (ATTO-DOPE) and blue (Cascade Blue) channels. Scale bars = 5 µm. **c)** Quantification of the NEC-mediated budding in the absence or the presence of peptides or UL25Δ44 Q72A. Budding was tested at 1:0.1, 1:0.3, 1:0.6, 1:1 or 1:10 molar ratios of NEC:UL25 or NEC:peptide. Each experiment was done in three biological replicates, each consisting of three technical replicates. Symbols represent average budding efficiency of each biological replicate relative to NEC220 (100%). Bars show the mean of three biological replicates, with error bars representing the standard error of the mean. Significance compared to NEC220 was calculated using an unpaired *t*-test. *P-value < 0.05, **P-value < 0.01, ***P-value < 0.001, and ****P-value < 0.0001.

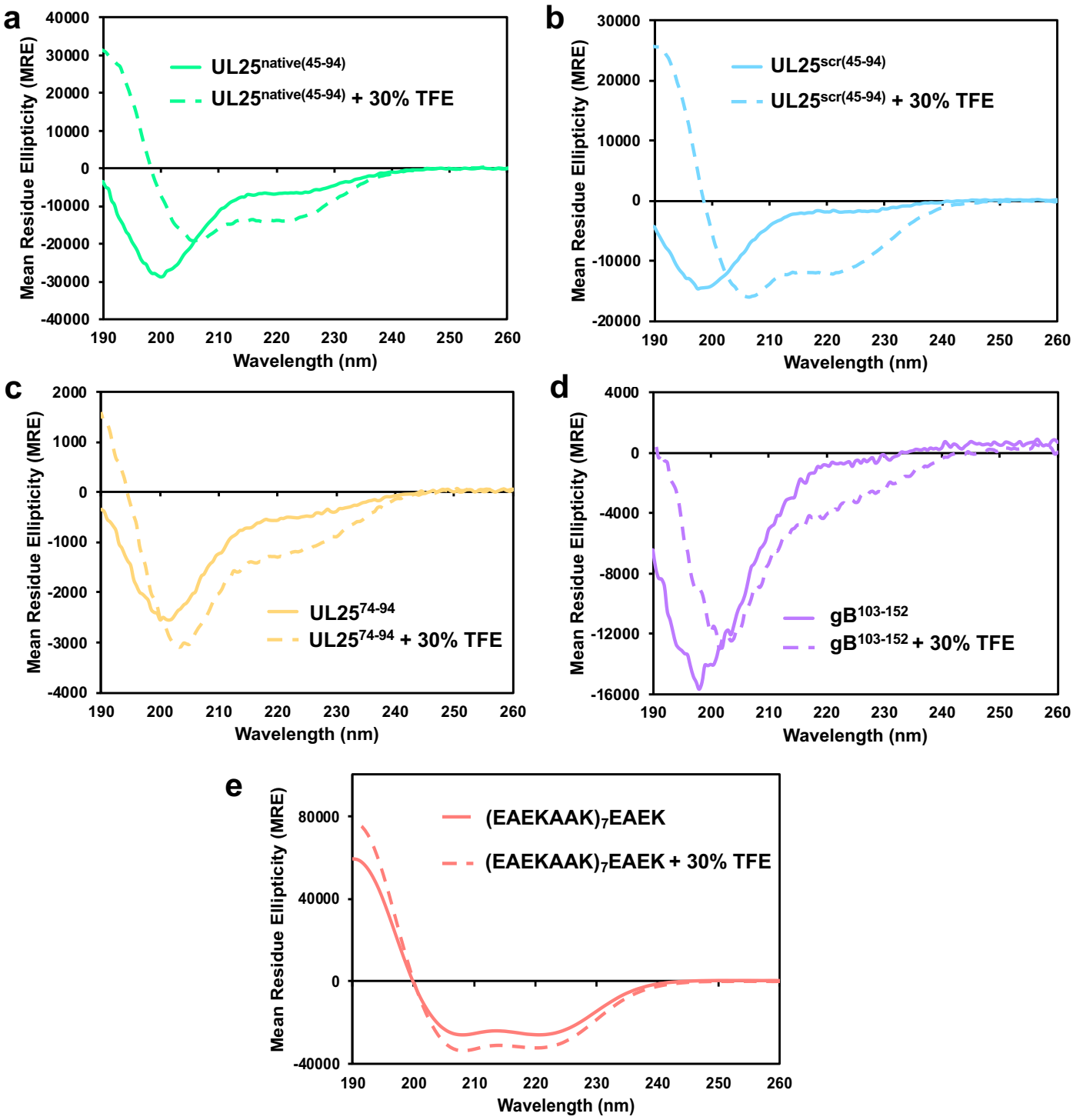

Figure 3. Secondary structure of the peptides used in this work. a-e) Far-UV CD spectra of each peptide in the presence of 30% TFE (dashed lines) or in its absence (solid lines). Both the UL25$^{native(45-94)}$ and the UL25$^{scr(45-94)}$ peptides form α-helices in the presence of 30% TFE. UL25$^{74-94}$ and gB$^{103-152}$ are mostly unstructured even in the presence of 30% TFE. The (EAEKAAK)$_7$EAEK peptide is α-helical regardless of the presence of TFE.

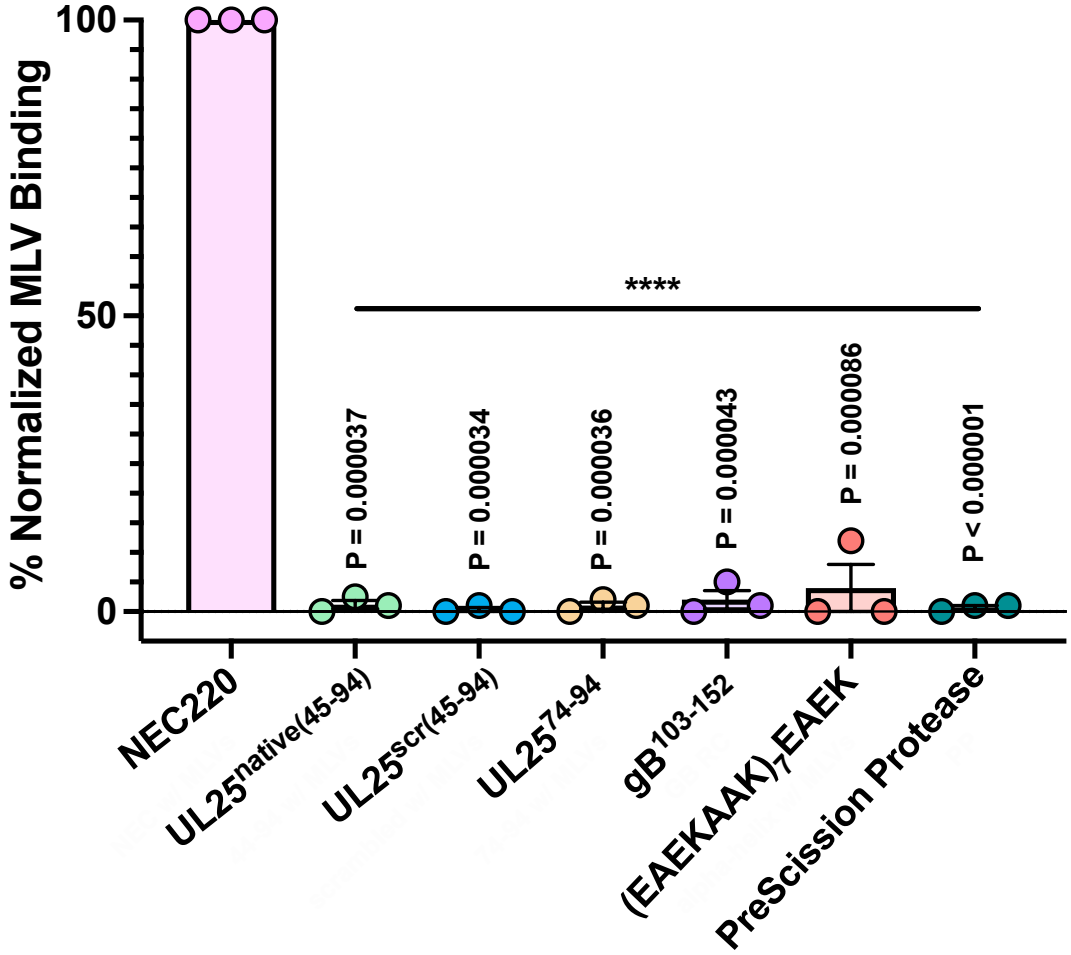

Figure 4. Peptides do not bind synthetic liposomes. NEC but not peptides bind multilamellar vesicles (MLVs) of the same composition as the GUVs used in the in-vitro budding assay. PreScission protease, which does not bind membranes, was used as a negative control. Each experiment was done in three biological replicates, each consisting of two technical replicates. Symbols represent average binding efficiency of each biological replicate relative to NEC220 (100%). Bars show the mean of three biological replicates, with error bars representing the standard error of the mean. Significance compared to NEC220 was calculated using an unpaired *t*-test. ****P-value < 0.0001.

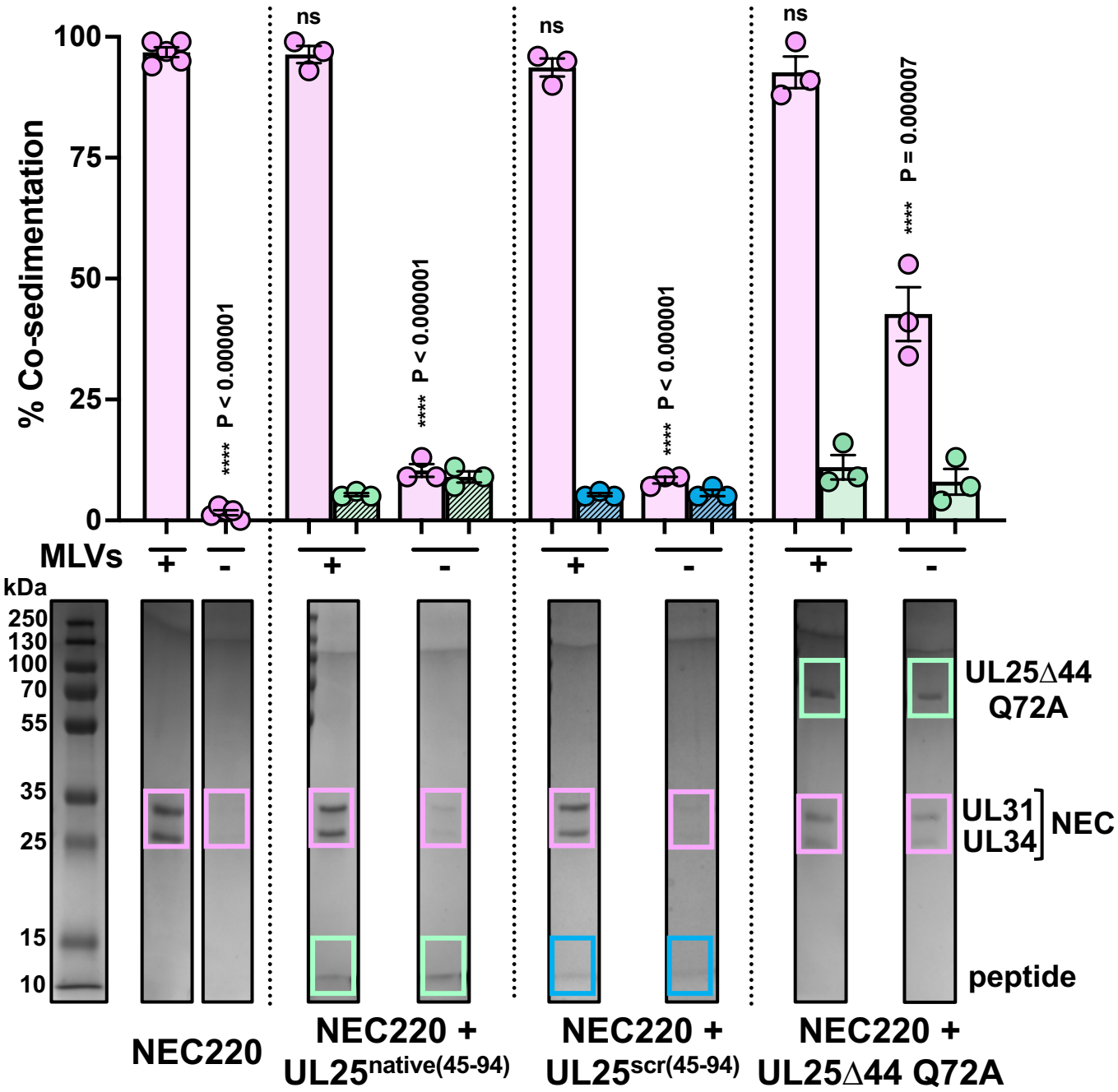

Figure 5. Peptides do not block membrane binding by the NEC. Co-sedimentation of NEC220 alone and in the presence of either UL25$^{native(45-94)}$, UL25$^{scr(45-94)}$, or UL25Δ44 Q72A was assessed by a co-sedimentation assay in the presence and absence of MLVs. The amount of co-sedimentation was quantified with Coomassie staining. Bands from cropped representative gels (full gel images are shown in Supplementary Figure 1) used for quantification are boxed and colored as follows: pink – NEC (UL31: 34 kDa and UL34: 25 kDa); green – either UL25$^{native(45-94)}$ (5 kDa) or UL25Δ44 Q72A (57 kDa); blue – UL25$^{scr(45-94)}$) (5 kDa). Each experiment was done in three biological replicates, each consisting of two technical replicates. Symbols represent average binding efficiency of each biological replicate. Bars show the mean of three biological replicates, with error bars representing the standard error of the mean. Significance compared to NEC220 in the presence of MLVs was calculated using an unpaired *t*-test. ****P-value < 0.0001.

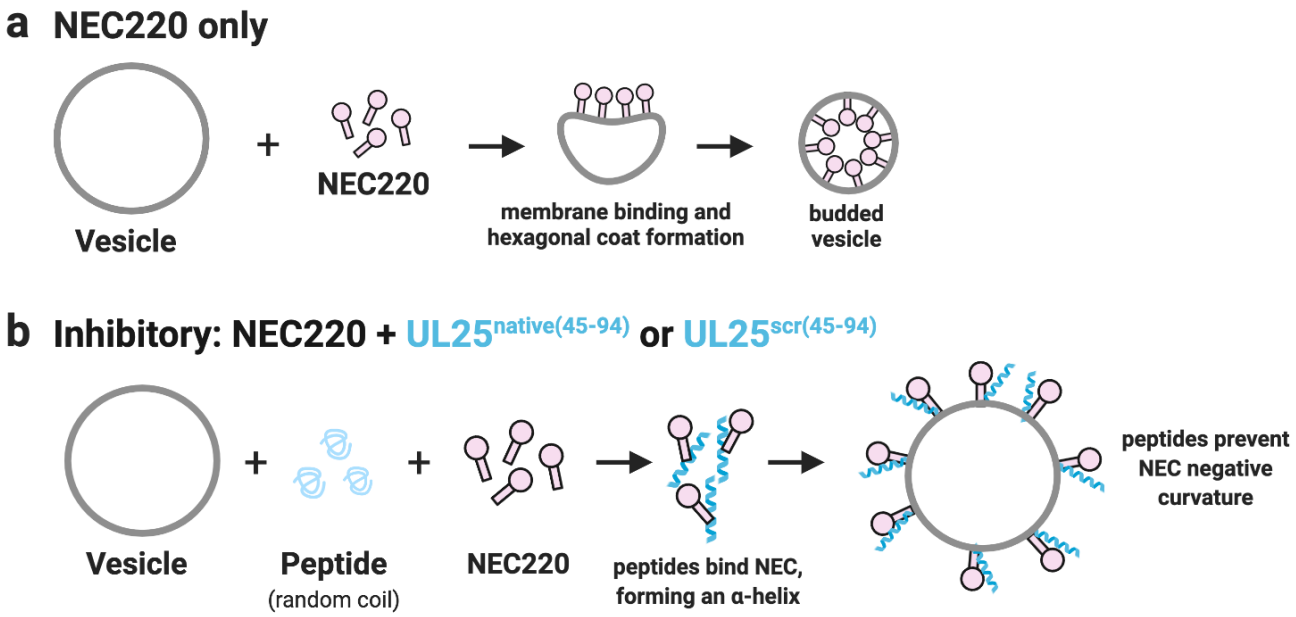

Figure 6. Proposed model of peptide inhibition of the NEC-mediated budding. a) NEC (pink) alone binds membranes, induces negative membrane curvature, and generates a budded vesicle containing an internal hexagonal NEC coat. **b)** Both UL25$^{native(45-94)}$ and UL25$^{scr(45-94)}$ (bluegreen) inhibit budding by forming α-helices upon binding to the NEC, which likely prevents conformational changes necessary for the formation of the negative membrane curvature. This figure was generated using Biorender (https://biorender.com).